Semiannual Progress Report
For 10/1/99-3/31/200:
Contract ID DE-AC26-99FT40714

Project Entitled:

"Optimization of the Cathode Long Term Stability in Molten Carbonate Fuel Cells: Experimental Study and Mathematical Modeling

Submitted to
Ms. Jo Ann Zysk, Contract Specialist
U.S. Department of Energy
National Energy Technology Laboratory
AAD Document Control, MS 921-107
P.O. Box 10940
Pittsburgh, PA 12236-06940

May 2000

Optimization of the Cathode Long Term Stability in Molten Carbonate Fuel Cells: Experimental Study and Mathematical Modeling

Anand Durairajan, Bala Haran, Branko N. Popov and Ralph E. White
Department of Chemical Engineering
University of South Carolina
Columbia, SC 29208

PART I. DEVELOPMENT OF HIGH PERFORMANCE CATHODE MATERIALS

INTRODUCTION

The cathode materials for molten carbonate fuel cells (MCFCs) must have low dissolution rate, high structural strength and good electrical conductivity. Currently available cathodes are made of lithiated NiO which have acceptable structural strength and conductivity.[1,2] However a study carried out by Orfeld et *al.*[3] and Shores et *al.*[4] indicated that the nickel cathodes dissolved, then precipitated and reformed as dendrites across the electrolyte matrix. This results in a decrease in cell utilization and eventually leads to shorting of the cell. The solubility of NiO was found to depend upon the acidity/basicity of the melt (basicity is directly proportional to log $P_{CO2)}$, carbonate composition, H_2O partial pressure and temperature. Urushibata *et al.*[5] found that the dissolution of the cathode is a primary life limiting constraint of MCFCs, particularly in pressurized operation. With currently available NiO cathodes, the goal of 40,000 hours for the lifetime of MCFC appears achievable with cell operation at atmospheric pressure. However, the cell life at 10 atm and higher cell pressures is in the range between 5,000 to 10,000 hours.

In order to resolve the NiO dissolution problem several different approaches were taken. These include (i) developing alternative materials for cathodes, (ii) using additives in the electrolyte to increase its basicity, (iii) increasing the fraction of Li in the baseline electrolyte, (iv) increasing the matrix thickness. Kucera *et al.* [6] showed that $LiFeO_2$ cathodes are chemically very stable. However, these electrodes have slow kinetics when compared with NiO at atmospheric pressure. The corrosion behavior of iron and chromium,[7] nickel-aluminum alloys,[8] nickel-chromium alloys[9] and aluminized stainless steel were studied in the eutectic containing 62 mol% Li_2CO_3 and 32% K_2CO_3 at 650^{o}C in presence of N_2(15 Vol %), O_2 (15 Vol%) and CO_2 (25 Vol %). Increased corrosion resistance was found in case of aluminized AISI 310 S.

According to Farooque[10] the cathode life can be increased by increasing the matrix thickness and by introducing an additive ($CaCO_3$) in the electrolyte. However, this approach caused an approximately 20 mV reduction in performance at 160 mA/cm^2.

Tanimoto *et al.*[11] and Ota *et al.*[12] increased the fraction of Li in the baseline electrolyte in order to create a milder cell environment than the base line electrolyte (62/38 Li/K). Also, additives such as $SrCO_3$ and $BaCO_3$ were used to increase the electrolyte basicity. Larger amount of these additives caused 20 to 30 mV reduction in performance of MCFC.

From the literature it is obvious that the dissolution of the cathode is the primary limiting factor for successful commercialization of MCFCs particularly in pressurized conditions. Several approaches to resolve the cathode dissolution can be investigated:

(i) to develop alternative material for the cathodes

(ii) to increase the matrix thickness,

(iii) to add additives in the melt which will increase the melt basicity.

The overall objective of this research is to develop a superior cathode for MCFC's with improved catalytic ability, enhanced corrosion resistance with low ohmic losses, improved electronic conductivity. We also plan to understand the corrosion processes occurring at the cathode/molten carbonate interface. The following cathode materials will be subjected to detailed electrochemical, performance, structural and corrosion studies.

(i) Passivated NiO alloys using chemical treatment with yttrium ion implantation and anodic yttrium molybdate treatment.

(ii) Novel composite materials based on NiO and nanosized Ce, Yt, Mo

(iii) Co doped $LiNiO_2$ ($LiNiO_2$ doped with 10 to 20% Co ($LiCo_{0.2}NiO_2$) and NiO cathodes.

(iv) CoO as a replacement for NiO.

Passivation treatments will inhibit corrosion and increase the stability of the cathode at high temperatures. Deposition of refractory metals (Mo, W, Li_2NiCrO_4) will impart stability to the cathode at high temperatures. Further it will also increase the electrocatalytic activity and corrosion resistance of the cathode. Doping with Co will decrease the alloy dissolution and increase the cycle life of the cathode.

Electrochemical characterization of the cathode materials under different operating conditions will include: (a) determination of the cathode polarization properties (current potential relationship), (b) polarization resistance and (c) exchange current density.

Using potentiostatic, galvanostatic and Electrochemical Impedance Spectroscopy (EIS) the transport properties of the electroactive species in molten carbonate melt and in the porous matrix of the cathode will be determined.

The corrosion properties of all cathode materials will be evaluated in molten carbonate melt using electrochemical techniques in combination with post-test analysis of quenched specimens. The objective will be to optimize the cathode composition and the chemical and anodic passivation treatments.

In the reporting period the oxidation behavior of Ni and Co in Li + Na carbonate eutectic was investigated under oxidizing environment using cyclic voltammetry, electrochemical impedance spectroscopy and potentiodynamic technique. The open circuit potential was monitored as a function of time in order to evaluate the material's reactivity in the melt.

EXPERIMENTAL

Electrode preparation: Finely ground powders of nickel and cobalt were mixed with a commercial plasticizer, disperser and binder in calculated amount of water solvent and were ball milled for 5-7 days. The slurry was then tape cast using a doctor blade assembly. The thickness of the matrix thus obtained was 1 mm and after sintering, the porosity was determined to be 53%. Gold wires were spot welded to the nickel and cobalt disc electrodes to serve as a current collector during electrochemical studies.

Electrochemical characterization: A schematic of the cell used for electrochemical characterization is shown in Figure 1.1. The electrochemical studies were carried out using a three-electrode set up with gold as the counter electrode and Au/($2CO_2$+O_2) as the reference electrode. The reference gas flow rate was maintained at 10 cc/min. Oxidant gas with a composition of 67% CO_2 and 33% O_2 was directly purged into the carbonate melt. All the electrochemical studies were done using an EG&G PAR model 273 potentiostat interfaced with a computer.

Material characterization: X-Ray diffraction analysis was used to study the different oxidation products formed during in-situ oxidation of the cathode plaque. The composition of the oxide phases was identified using EPMA

RESULTS AND DISCUSSION

Open Circuit Potential Studies. To evaluate the oxidation properties of Ni and Co in the eutectic melt, the open-circuit potentials of both metals were monitored as a function of time under the oxidant composition of 67% CO_2 and 33% O_2. Figure 1.2 shows the OCP behavior of nickel electrode as a function of immersion time. Similar response was obtained for the cobalt electrode.

Three different potential plateaus were observed in case of Ni oxidation before reaching the oxygen redox potential. The observed plateaus have been attributed in the literature to the following reactions:[13,14]

$$Ni + CO_3^{2-} \rightarrow NiO + CO_2 + 2e^- \qquad \text{-0.80 V}$$

$$2Ni + 3CO_3^{2-} \rightarrow Ni_2CO_3 + 3CO_2 + 2e^- \qquad \text{-0.43 V}$$

$$Ni + CO_3^{2-} \rightarrow NiCO_3 + 2e^- \qquad \text{-0.25 V}$$

$$(1-x)Ni(II)O + xLi + xCO_3^{2-} \rightarrow Li_xNi(II)_{1-2x}Ni(III)_xO + xCO_2 + xe^-$$

Similar redox processes have been suggested for the oxidation of cobalt in the carbonate electrolyte under oxidant gas conditions.[13,14]

$$Co + CO_3^{2-} \rightarrow CoO + CO_2 + 2e^- \qquad \text{-0.85 V}$$

$$2Co + 4CO_3^{2-} \rightarrow Co_3O_4 + 4CO_2 + 8e^- \qquad \text{-0.68 V}$$

$$Co + CO_3^{2-} \rightarrow CoCO_3 + 2e^- \qquad \text{-0.35 V}$$

$$CoO + Li^+ + CO_3^{2-} \rightarrow LiCoO_2 + CO_2 + e^-$$

The first plateau in case of nickel oxidation is due to the formation of porous nickel oxide on the surface of the nickel matrix. Oxygen diffuses through the porous oxide layer and gradually oxidizes the bulk nickel to NiO at approximately –0.6 V. The second plateau at –0.44 V has been attributed to the surface oxidation of Ni(II) oxide to trivalent nickel. Next, the lithiation of the oxide occurs at this or at more positive potentials. The inclusion of lithium in the bulk of the oxide increases the conductivity of the cathode matrix by 5-6 times.[13] XRD patterns presented at the end of this work indicated the presence of small amount of a lithiated compound $LiNO_2$. Further studies are necessary in order to explain the lithiation reaction mechanism.

Cyclic voltammetry studies

To study the oxidation and reduction processes occurring at the electrode electrolyte interface in further detail, cyclic voltammetry studies were carried out on Ni and Co electrodes at different times of immersion. In the first set of studies the potential of the Ni electrode was swept from –1.0 V to 0 V and then reduced back to –1.0 V using a scan rate of 50 mV/sec. Figure 1.3 shows the CV response of Ni electrode at different times of immersion in the melt. Initially, at small immersion times, the current during the anodic sweep (close to –0.1 V) is very high due to the enormous amount of nickel available at the surface for oxidation. As soon as NiO is formed on the surface, the oxidation of the bulk Ni proceeds slowly. The reduction peaks increase during the reverse sweep indicating the availability of more NiO for reduction. An interesting feature of the CVs is the shift in the reduction peak with increase in the time of immersion in the melt. In order to understand this behavior a second set of CVs were obtained on the Ni electrode in the same melt.

Figure 1.4 shows the CVs obtained on Ni at different times of immersion. In Fig. 1.3, the potential was scanned from –1 to 0 V with respect to the reference electrode. However, in Fig. 1.4 the potential was swept 250 mV above and below the rest potential of the electrode. Initially the anodic currents are large signifying oxidation of the surface Ni. However the current

decreases as the surface is covered with more and more NiO. After the formation of dense NiO layer, the oxidation current significantly decreases. Oxygen reduction reaction was observed during the reverse peak after the electrode is completely oxidized. Since, the potential of the electrode changes with time of immersion the CVs shift towards more positive potentials with time.

Impedance analysis: Electrochemical impedance spectroscopy studies were carried out on nickel and cobalt electrodes at regular intervals during in-situ oxidation. Figure 1.5a shows the Nyquist plots of the impedance response on Ni at different times of oxidation. As shown in this plot, the cathode resistance increases with time due to the NiO film growing. Similar dependence was observed in case of cobalt due to CoO formation. At higher overpotentials, the resistance starts to decrease due to the lithiation process, which takes place at the interface. The amount of Li in the matrix has not been yet determined by any analytical technique because of its low concentration. NiO and CoO are supposed to behave like p-type semiconductor. Insertion of Li^+ instead of oxygen atom induces vacant spots (holes), which are responsible for ionic conduction.

Figure 1.5b compares the impedance data obtained for fully formed nickel and cobalt oxide electrodes. It is seen in Fig. 5b that the cobalt electrode has higher conductance than the nickel electrode. The observed difference can be explained by taking into account that the conductivity of the cobalt either results from the higher lithium content in the oxide matrix or from the intrinsic conductivity of cobalt metal.

The improvement in electrocatalytic ability of the cobalt oxide over the nickel oxide is shown in Figure 1.6. As shown in this figure, higher cobalt oxide reduction current is observed when compared with the of nickel oxide reduction current (formed after 8 hours of immersion) indicating better ability of the cobalt oxide to serve as a catalyst for oxygen reduction.

Surface Characterization: Ni matrix was analyzed for the oxide products by EPMA and XRD at two different times of immersion. EPMA analysis done on sample oxidized for 4 hours showed a complete coverage of the surface with bivalent nickel oxide species. The atomic percentage of nickel and oxygen clearly suggested the presence of NiO species on the surface. Sample taken after complete oxidation, on the other hand, showed the presence of more than one phase of NiO. Significant amount of trivalent nickel oxide were also seen on the surface. This agrees with the oxidation processes described before. The elemental mapping done on these

samples are shown in Figure 1.7. As it is shown in the figure, completely oxidized Ni, clearly shows the presence of two phases of nickel oxide. Lithium could not be quantitatively estimated using this technique.

Figure 1.8 shows the results of XRD analysis performed on nickel samples after 4 hours of oxidation and after a complete oxidation. As seen in this figure, the sample after four hours of oxidation shows a presence of Ni (II) oxide phase. However, upon further oxidation, a trivalent nickel oxide is formed. The presence of $LiNiO_2$ in the sample is uncertain.

REFERENCES

1. K. Kinoshita, F. Mc.Larnon, and E. Cairns, *Fuel Cells, A Handbook,* prepared by Lawrence Berkeley Laboratory for the U.S. Department of Energy, May 1988.
2. N. Minh, "High Temperature Fuel Cells," *CHEMTECH,* **21,** 32, (1991).
3. M. L. Orfield and D. A. Shores, *Corrosion 86,* paper No 88, National Association of Corrosion Engineers, Houston, TX, 1986.
4. D. A. Shores, *Proceedings of the 22nd Intersociety Energy Conversion Engineering Conference,* **2**, 1023, American Institute of Aeronautics and Astronautics, New York, p. (1987).
5. H. Urushibata and T. Murahashi, MELCO, "Life Issues of Molten Carbonate Fuel Cell," in *The International Fuel Cell Conference Proceedings,* NEDO/MITI, Tokyo, Japan, p. 223-226, (1992).
6. G. Kucera, K. Myles, A. Brown, M. Roche, D. Chu, and E. Indacochea, "ANL's Research and Development of Alternate Components for MCFCs," *Proceedings of the Fourth Annual Fuel Cell Contractors Review Meeting,* U.S. DOE/METC, p. 31-41, July (1992).
7. M. Spiegel, P. Biedenkopf and H. J. Grabke, *Corrosion Science,* **39**, 1193 (1997).
8. J. P. T. Vossen, R. C. Makkus, A.H.H. Jansen, J. H. W. deWit, *Materials and Corrosion-Wekstoffe und Korrosion,* **48**, 228 (1997).
9. J. P. T. Vossen, R. C. Makkus, A.H.H. Jansen, J. H. W. deWit, *Materials and Corrosion-Wekstoffe und Korrosion,* **48**, 157 (1997).
10. K. Matsumoto, A. Matsuoka, K. Nakagawa, *Denki Kagaku,* **66**, 537 (1998).
11. M. Faroque, ERC, "Development on Internal Reforming Carbonate Fuel Cell Technology," Final Report, US DOE/METC, DOE/MC/23274-2941, Pgs.3-18, (1990).

12. K. Tanimoto, International Fuel Cell Conference Proceedings, NEDO/MITI, Japan, p. 185, (1992).
13. P Tomczyk, H Sato, K Yamada, T Nishina and I Uchida, *J. Electroanal. Chem.*, 391 p133 (1995).
14. B Y Yang and K Y Kim, *Electrochim. Acta,* **43**, p. 3343 (1998)

PART II. DEVELOPMENT OF CORROSION RESISTANT CURRENT COLLECTORS

Bipolar plates and the current collectors, which are both, made of stainless steel or nickel alloys undergo severe corrosion under MCFC operating conditions.[1-3] Current research attempts to improve the corrosion resistance of these components involves applying a coating that protects the underlying steel against corrosion.[4-5] To reduce the corrosion on the anode side, a nickel electro cladding has been used. However, nickel does not offer good barrier protection to the diffusion of oxygen. Coating with aluminum has been reported to improve the corrosion resistance and give lifetime corrosion protection in the wet-seal area. However, the high electrical resistance of an Al_2O_3 or $LiAlO_2$ scale is not acceptable for practical use in MCFCs.[6]

The separator plates are made from Fe-Ni-Cr austenitic stainless steels 310S, 316 or 316L. These materials contain a sufficient amount of chromium to form a protective oxide layer, which prevents any oxidation process to occur on the material.[7] However, the chromium layer slowly reacts with the carbonate melt leading to a loss of the electrolyte. Dissolutions of chromium from the alloy results in an increase of the corrosion rate as well as in increase of the ohmic loss due to the formation of corrosion products on the steel. Thus in order to increase the corrosion resistance of the current collector, it will be necessary to develop novel coatings, which possess barrier properties to the diffusion of oxygen. Also, the coating should restrict the outward diffusion of steel components, which is a common problem associated with the Ni coatings.

In order to improve the current collector barrier properties and its electronic conductivity we suggest (i) to develop composite coatings of nanolayers of Co-P, Co-Mo, Ni-P, Ni-Mo, Co-Ni, Co-SiO_2 –Ni-SiO_2 or Ni-Co-P over carbon steel and stainless steel, (ii) to develop Fe-Al cast alloys with different composition, (iii) to use in-house developed treatment for depositing nanolayers of W, Mo, and Ce on stainless steel.

The specific objectives for developing a superior current collector are:

(i) Development of nanostructured composite coatings over steel substrate (Co-P, Co-Mo, Ni-P, Ni-Mo, Co-Ni, Co-SiO_2 –Ni-SiO_2 or Ni-Co-P).

(ii) Preparation of cast alloys FeAl doped with Co or Mo and binary nickel aluminides,

(iii) Surface modification of FeAl and binary nickel aluminides by electrodeposition of thin films of Mo, W or Li_2NiCrO_4 using in house developed treatments from molten LiCl-KCl eutectic melt.

(iv) Construction of molten salt cell for corrosion and electrochemical characterization of cathode materials in molten carbonates at 650^{o}C,

(v) Electrochemical characterization of the cathode materials under different operating conditions which includes; (a) determination of the cathode polarization properties (current potential relationship), (b) polarization resistance and (d) exchange current density

(vi) Determination of the corrosion rates of the cathode materials under different operating conditions.

(vii) Development of nanostructured composite coatings over steel substrate

(viii) Preparation of cast alloys FeAl doped with Co or Mo and binary nickel aluminides,

Before depositing nanostructured amorphous composite coatings of Co-P, Co-Mo, Ni-P, Ni-Mo, Co-Ni, Co-SiO_2 –Ni-SiO_2 or Ni-Co-P on steel initially it was necessary to investigate the corrosion properties of SS 304 under simulated cathode gas environment conditions and to evaluate the corrosion processes occurring at different overpotentials. Next, in-house developed treatment will be used for deposition of nanostructured amorphous composite coatings with superior barrier properties.[8]

EXPERIMENTAL

The corrosion and kinetic studies were carried out using standard electrochemical testing techniques. The faradaic parameters, which control the rate of oxygen reduction and the corrosion rates were determined using linear polarization technique, Tafel technique, Cyclic Voltammetry (CV) and Electrochemical Impedance Spectroscopy. A variety of material characterization techniques (Raman spectroscopy, EDAX, XRD, SEM) are used to monitor the corrosion products. The various alloy constituents dissolved in molten carbonate melt are determined using AA and Ion Chromatography.

Electrodes of area 1 cm^2 were made from a perforated stainless steel 304 (Perforated Metals Inc.), with a void area of 45%. Gold wires were spot welded to the flat electrodes and served as a current collector during the electrochemical studies.

A schematic of the cell used for electrochemical characterization and corrosion studies is shown in Figure 1.1. Electrochemical studies were carried out using a three-electrode set up with gold as the counter electrode and Au/($2CO_2$+$1O_2$) as the reference electrode. The reference gas flow rate was maintained at 10 cc/min. Oxidant gas with a composition of 67% CO_2 and 33% O_2 was directly purged into the carbonate melt. All the electrochemical studies were done using an EG&G PAR model 273 potentiostatic interfaced with a computer. SEM was used to characterize the morphology changes during the oxidation of the SS 304.

RESULTS AND DISCUSSION

Cyclic voltammetry: CV's were obtained between –1.6 and –0.15 V on substrates exposed at different times in the carbonate eutectic melt. The sweep rate was 50 mV/s. Figure 2.1a shows CV's obtained after 0.5 h and 15 h of exposure of the samples under cathode gas atmosphere in the Li/Na carbonate melt. Figures 2.1b and 2.1c show the CV responses between –1.6 V and –0.8 V and between –1.2 V and –0.6 V *vs.* Au/$2CO_2$+$1O_2$ reference electrode, respectively.

The 304 stainless steel forms multiple corrosion products with mixed compositions.[9-14] The observed peak potentials of 304 stainless steel are labeled as A through E in Figure 2.1. Peak A observed at –1.1 V vs. Au reference electrode corresponds to the oxidation of Fe to FeO and $LiFeO_2$ according to the following oxidation reactions:

$$Fe + CO_3^{2-} \leftrightarrow FeO + CO_2 + 2e^- \qquad E = -1.1\ V\ (E_o = -1.11\ V)$$

Peak B observed at –0.85 V corresponds to formation of $LiFeO_2$

$$\frac{2}{3}Fe + \frac{2}{3}Li^+ + \frac{4}{3}CO_3^{2-} \leftrightarrow \frac{2}{3}LiFeO_2 + \frac{4}{3}CO_2 + 2e^- \qquad E = -0.85\ V\ (E_o = -1.40\ V)$$

At more positive potentials than –0.7 V, the current continuously increases up to –0.2 V. The observed increase in current is due to the oxidation of iron, nickel and chromium through the following reactions:

$$2FeO + 2Li^+ + 2CO_3^{2-} \leftrightarrow 2LiFeO_2 + 2CO_2 + 2e^- \qquad E = -0.6\ V\ (E_o = -0.78\ V)$$

$$4Fe + LiFeO_2 + 6CO_3^{2-} \leftrightarrow LiFe_5O_8 + 6CO_2 + 12e^- \qquad E = -0.6\ V\ (E_o = -0.60\ V)$$

$$Ni + CO_3^{2-} \leftrightarrow NiO + CO_2 + 2e^- \qquad E = -0.6\ V\ (E_o = -0.81\ V)$$

$$\frac{1}{3}Cr + \frac{4}{3}CO_3^{2-} \rightarrow \frac{1}{3}CrO_4^{2-} + \frac{4}{3}CO_2 + 2e^- \qquad E = -0.2\ V\ (E_o = -0.42\ V)$$

Li_2CrO_4 is a thermodynamically stable product in molten carbonates. However, it is not stable as a passivation layer and dissolves in the melt as chromate ions. In the reverse scan reduction of $LiFeO_2$ to FeO and reduction of NiO to Ni occur (peaks D and E) according to the following reduction processes:

$$LiFe_5O_8 + 4e^- \rightarrow LiFeO_2 + 4FeO + 2O_{sol}^{2e-} \qquad E = -0.8V$$

$$NiO + 2e^- \rightarrow Ni + O_{sol}^{2e-} \qquad E = -1.0V$$

$$LiFeO_2 + 4e^- \rightarrow FeO + Li^+ + O_{sol}^{2e-} \qquad E = -1.0\ V$$

As shown in Figure 2.1a, the current density increases considerably with increasing the sample exposure time. Also, the peak potentials shift in positive direction. The results indicated that oxide layers are formed on the surface, which induce anodic potentials, increase the porosity and consequently increase the surface area and the corrosion rate.

The observed potential plateaus in this study indicated a growth of different passive layers on stainless steel. In the potential range between –1.0 V and 0.0 V *vs.* Au reference electrode, iron is oxidized to FeO and $LiFeO_2$, nickel is oxidized to $LiNiO_2$ and trivalent nickel oxide, while chromium is oxidized to $LiCrO_2$ and $LiCrO_4$. Thus, the surface composition of the alloy strongly determines the open circuit potential, the conductivity and the ohmic drop at the interface with the electrolyte.

Corrosion studies under open circuit conditions: Figure 2.2 shows the open circuit potential of 304 steel as a function of exposure time in Li + Na carbonate melt under cathode gas environment. The first potential shift observed in Figure 2.2 is caused by the surface oxidation of the sample. Chromium oxidizes faster than iron and nickel resulting in the surface to contain mainly oxides of chromium. Oxidation of chromium causes a shift to more positive potentials. It also increases the porosity and consequently increases the surface area and the iron corrosion rate. Thus, the second potential shift is due to the formation of $LiFeO_2$. The $LiFeO_2$ layer is porous and facilitates more dissolution of the underlying chromium.

Tafel Polarization Studies: Tafel polarization technique was used to estimate the corrosion rates of 304 steel at different exposure times (after 1, 8 and 15 hours). The sweep rate was 5 mV/sec.

Table I summarizes the total surface resistances (R_p) and corrosion current densities determined at different exposure times. As shown in Table I, the surface resistance rapidly increases with time due to more amount of oxide formation. The oxidant gas available for cathodic reaction was kept low in order to minimize the effect of oxygen reduction reaction.

Table I. Corrosion rates of SS 304 measured at different immersion times in carbonate eutectic melt

Time (hours)	OCP (V vs. $Au/2CO_2+1O_2$)	i (A/m^2)	R_p (Ω)
1	-0.940	0.0640	1380
8	-0.422	0.0120	8.2E 4
15	-0.0025	0.0009	1.0E 5

Surface Analysis: Surface analysis of fresh and oxidized (under cathodic conditions) SS 304 were carried out using EDAX and SEM methods. EDAX analysis of the surfaces given in Figures 2.3a and 2.3b show chromium and nickel deficient areas in case of the fresh and oxidized sample, respectively. Fresh sample has relatively higher concentration of nickel and chromium at the surface. Chromium oxidizes under cathodic conditions in MCFC and dissolves into the melt. The chromium oxides depletion from the surface leads to diffusion of more chromium from the bulk and subsequent oxidation. Underlying iron and nickel oxidize and the oxides later react with the lithium in the melt to form a lithiated compound, which explains our observation of higher iron content and lower chromium content in the surface in the case of oxidized sample. Figure 2.4 shows the SEM micrographs of the oxidized and fresh samples. Presence of oxidized layers is clearly seen in the case of 304 steel immersed in melt for 24 h.

CONCLUSIONS

In the reporting period the oxidation behavior of Ni and Co in Li + Na carbonate eutectic was investigated under oxidizing environment using cyclic voltammetry, electrochemical

impedance spectroscopy and potentiodynamic technique. The open circuit potential was monitored as a function of time in order to evaluate the materials reactivity in the melt.

The results indicated that nickel oxidation occurs through formation of porous nickel oxide on the surface of the nickel matrix. At higher overpotentials, oxidation results in formation of trivalent nickel oxides. The XRD patterns indicated the presence of small amount of a lithiated compound $LiNO_2$. Further studies are necessary in order to explain the lithiation reaction mechanism.

Electrochemical impedance spectroscopy indicated that the Ni cathode resistance increases with time due to the formation of NiO film on the surface. Similar dependence was observed in case of cobalt due to CoO formation. At higher overpotentials, the resistance starts to decrease due to the lithiation process, which takes place at the interface. The amount of Li in the matrix has not been yet determined by any analytical technique because of its low concentration. NiO and CoO are supposed to behave like p-type semiconductor. Insertion of Li^+ in lieu of oxygen atom induces vacant spots (holes), which are responsible for ionic conduction. The cobalt electrode has higher conductance than the nickel electrode. The observed difference can be explained by taking into account that the conductivity of the cobalt either results from the higher lithium content in the oxide matrix or from the intrinsic conductivity of cobalt metal.

EPMA analysis done on Ni sample oxidized for 4 hours showed a complete coverage of the surface with bivalent nickel oxide species. The atomic percentage of nickel and oxygen clearly suggested the presence of NiO species on the surface. Sample taken after complete oxidation, on the other hand, showed the presence of more than one phase of NiO. Significant amount of trivalent nickel oxide were also seen on the surface. This agrees with the oxidation processes described before. The elemental mapping done on these samples clearly shows the presence of two phases of nickel oxide. Lithium could not be quantitatively estimated using this technique.

The corrosion properties of SS 304 were investigated under simulated cathode gas environment condition. The corrosion products formed at different overpotentials were identified using EDAX and the thermodynamic redox potentials.

The corrosion and kinetic studies were carried out using standard electrochemical testing techniques. The faradaic parameters, which control the rate of oxygen reduction and the corrosion rates were determined using linear polarization technique, Tafel technique, Cyclic

Voltammetry (CV) and Electrochemical Impedance Spectroscopy. A variety of material characterization techniques (Raman spectroscopy, EDAX, XRD, SEM) were used to monitor the corrosion products.

The results indicated that chromium in the alloy oxidizes faster than iron and nickel resulting in the surface to contain mainly chromium oxides. Oxidation of Cr to chromium oxides induces anodic overpotentials, increases the porosity of the surface layer and consequently increases the surface area and the iron corrosion rate. The corrosion of iron results in formation of $LiFeO_2$ layer which is porous and facilitates more dissolution of the underlying alloy.

FUTURE WORK

The overall objective of this research is to develop a superior cathode for MCFC's with improved catalytic ability, enhanced corrosion resistance with low ohmic losses, improved electronic conductivity and to understand the corrosion processes occurring at the cathode/molten carbonate interface. In the future, the following cathode materials will be subjected to detailed electrochemical, performance, structural and corrosion studies: (i) novel composite materials based on NiO and nanosized Co, Ce, Yt, or Mo and (ii) CoO as a replacement for NiO.

Passivation treatments will inhibit corrosion and increase the stability of the cathode at high temperatures. Deposition of refractory metals will impart stability to the cathode at high temperatures. Further it will also increase the electrocatalytic activity and corrosion resistance of the cathode. Doping with Co will decrease the alloy dissolution and increase the cycle life of the cathode.

Currently, detailed electrochemical structural and corrosion studies are being done to characterize the corrosion properties of 304 stainless steel and of 304 steel coated with nanostructured amorphous composite layers of Co-P, Co-Mo, Co-Ni, Ni-P or Ni-Mo-P. The composite layers are formed using in-house electrocatalytic process, which will be described in our next report. The corrosion studies are carried out using a three-electrode cell shown in Figure 2.1 as well as laboratory 3-cm^2 fuel cell (Figure 3). Electrochemical characterization of the cathode materials under different operating conditions will include: (a) determination of the cathode polarization properties (current potential relationship), (b) polarization resistance and (d)

exchange current density and (e) determination of the corrosion rates of the cathode materials under different operating conditions.

All experiments will be conducted in a symmetrical in-house 3 cm^2 unit cell as shown in Fig. 3. The cell configuration is circular and the incoming gas flows through the orifices in the current collectors, perpendicularly to the electrode. The inner diameter of outer alumina tube is about 1 in. The current collector for cathode gas was made of 316L stainless steel (SUS) perforated sheet metal and 304S SUS rod. The upper outer tube is under appropriate pressure and contacts with the edge of the matrix making a wet seal.

The current collector for anode is pure nickel (Ni). Inner alumina tube in anode side was actually extended all the way up to support the cathode current collector. The end of both inner tubes has slots for gas flow. The reference electrode was extended to the bottom of the well in the collar. $LiAlO_2$/carbonate mixture will be placed in the bottom of the well to raise the level above the capillary hole. The reference electrode will be fed with a gas mixture of 33% oxygen (O_2) and 67% carbon dioxide (CO_2). The diameter of well is about 0.25 in and that of reference electrode is about 0.24 in. The lab-scale unit cell will be placed in a dc furnace and held at 650 ^oC during cell operation by a temperature controller.

APPENDIX

Construction of Cell Components shown in Fig. 3: γ-$LiAlO_2$ (Chemetall HSA10) was mainly used as a ceramic matrix and small amount of LSA50 was added into HAS10 to increase mechanical strength of the matrix.

To make a ceramic matrix tape, γ-$LiAlO_2$ was dried overnight at 110 ^oC and ball milled with 10 wt% dibutyl phthalate (DBP, Aldrich), 0.5 wt% corn oil deflocculant (Imperial Solsperse-9000) in an azeotropic mixture of toluene and ethanol (68/32) for 24 hrs. Next, polyvinyl butyral binder (PVB, Solutia Com, Butvar 76) was added into the slurry and then ball milled for 72 hrs. The slurry was vacuumed in a rotary evaporator in order to eliminate bubbles. The viscosity was maintained around 15,000 cp. Then the slurry was cast onto Mylar film (glycol terephthalic acid polymer) using a doctor blade. The ceramic matrix shows high dimensional stability without crack after 650 ^oC sintering. The 0.25 μm of average pore size and 60% of porosity was obtained by the mercury intrusion method (Micromeritics model 9220). The thickness of ceramic matrix film was about 0.5 mm.

Carbonate electrolyte was a mixture of Li_2CO_3/K_2CO_3 (62/38 m/o). The carbonate powders were mixed with DBP plasticizer, acrylic copolymer deflocculant (BYK-Chemie USA Inc., Disperbyk-110) in ethanol for 24 hrs and then PVB binder (Solutia B30H) was added into the slurry. The viscosity of slurry was 6,000 to 7,000 cp after de-airing by rotary evaporator.

Ni + 10 w/o Cr anode sheet was made of Ni powder (Inco Carbonyl-nickel type 255) and Cr powder (Alfa). Both metal powders were mixed with methyl cellulose binder and glycerin plasticizer in water and then casted onto Mylar carrier film after de-airing of the slurry. The anode matrix was sintered at 1000 ^oC for 30 min in a mixture of Ar/H_2 (90/10) atmosphere. The thickness of final matrix was about 0.7 mm, and also the pore size and porosity were about 3 to 4 μm and 50%, respectively.

Ni powder (Inco type 255) was used as a cathode. Ni was converted to lithiated NiO in MCFC by in-situ oxidation and lithiation. The tape casting procedure is just same to the case for anode but cathode matrix was sintered at 700 ^oC for 30 min. The thickness of final matrix was about 0.65 mm. The pore size and porosity were about 8 to 9 μm and 70 to 80%, respectively.

REFERENCES

1. M. Keijzer, G. Lindbergh, K. Hemmes, P.J.J. M. van der Put, J. Schoonman and J. H. W. de Wit, *J. Electrochem. Soc.*, **146**, 2508 (1999).
2. P. Biedenkopf, M. Spiegel, and H. J. Grabke, *Mater Corr.*, **48**, 477 (1997).
3. P. Biedenkopf, M. Spiegel, and H. J. Grabke, *Mater Corr.*, **48**, 731 (1997)
4. J. M. Fisher and P. S. Bennet, *J. MaterSci.*, **26**, 749 (1991)
5. M. Sasaki, S. Ohta and N. Igata, *Corr. Eng. ,* **45**, 215 (1991).
6. M. Okuyama, A. Tsurumu, Y. Itoi and S. Kamble, in *Proceedings of the 11th International Corrosion Congress*, Florence Vol 4, p 495 (1990).
7. M. S. Yazici and J. R. Selman, in *Carbonate Fuel Cell Technology IV,* J.R. Selman, I. Uchida, H. Wendt, D. A. Shores and T. F. Fuller, Editors, PV 97-4, p 253, The Electrochemical Society Proceedings Series, Pennington, NJ (1997)
8. A. Durairajan, B. S. Haran, R. E. White and B. N. Popov, *J. Power Sources,* **87**, 84, (2000).
9. J B J Veldhuis, S B Van der Molen, R C Makkus and G H J Broers, *Ber. Bunsenges. Phys. Chem.,* **94** (1990) 947
10. R D Pierce, J L Smith and G H Kucera, *Prog. Batteries Solar Cells*, **6** 159 (1987).
11. K Ota, S Mutsushima, S Kato, S Asano, H Yoshitake and N Kamiya, *J. Electrochem. Soc.*, **139** 667 (1992).
12. K Scott, M P Yang and J Winnick, *J. Electrochem. Soc.*, **130** (1983) 527
13. L Plomp, E F Sitters, C Vessies and F C Eckes, *J. Electrochem. Soc.*, **138** (1991) 629
14. P Tomczyk, H Sato, K Yamada, T Nishina and I Uchida, *J. Electroanal. Chem.,* **391** p133 (1995)

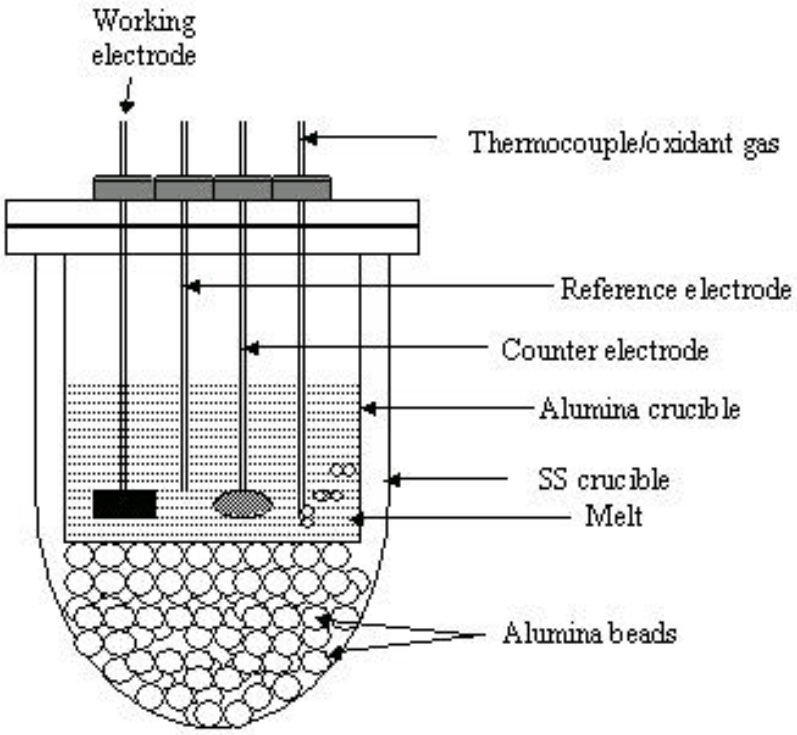

Figure 1.1 Schematic of a lab-scale electrochemical cell used for MCFC studies

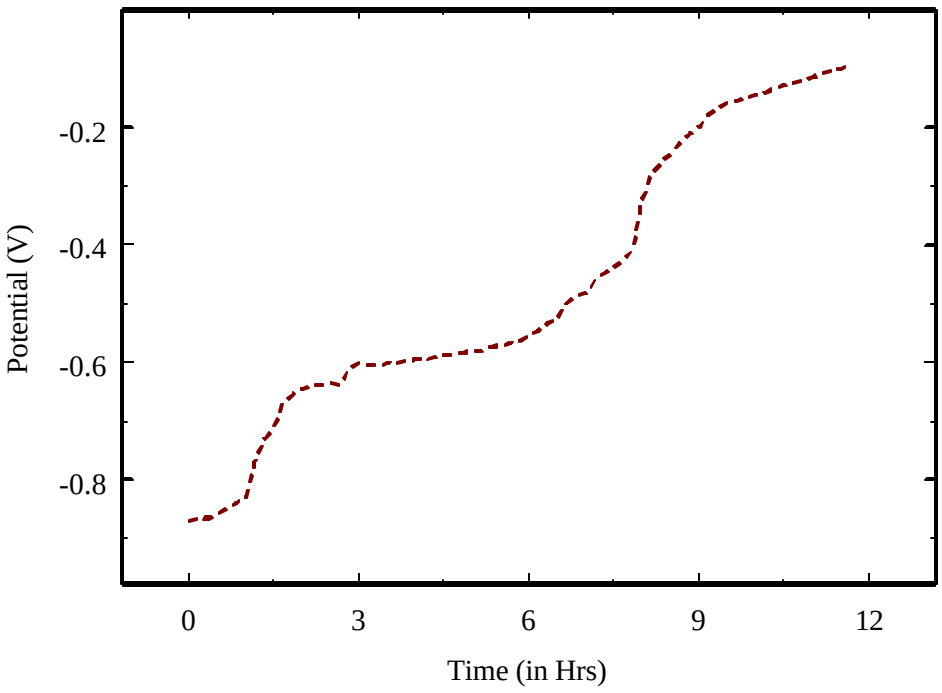

Figure 1.2 Open circuit potential of nickel electrode as a function of immersion time in Li + Na carbonate eutectic melt at 650 ^{o}C

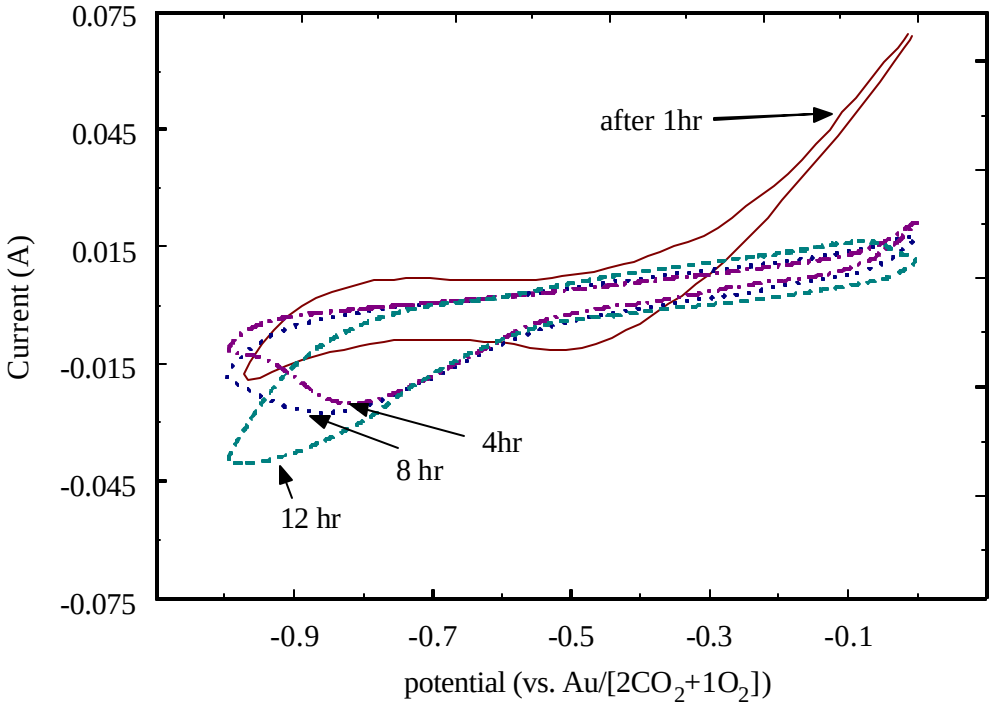

Figure 1.3 Cyclic voltammograms of nickel electrode immersed in Li + Na carbonate eutectic melts after different immersion times. Potential was scanned from –1.6 V to 0 V at a rate of 50 mV/sec.

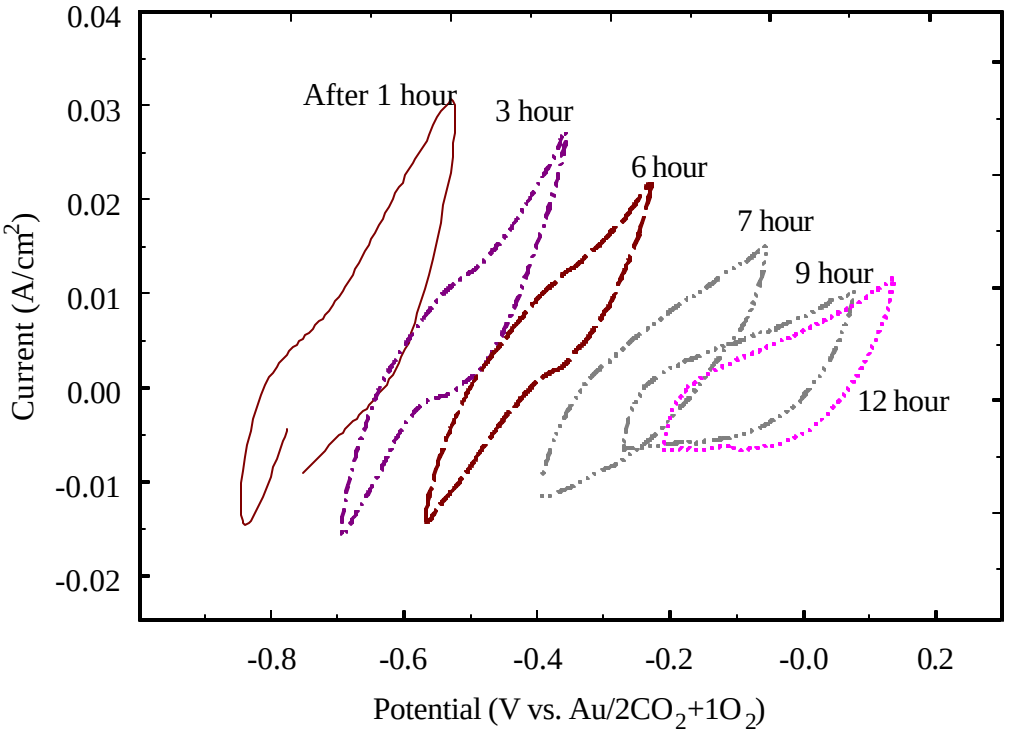

Figure 1.4 Cyclic voltammograms of nickel electrode immersed in Li + Na carbonate eutectic melts after different immersion times. Potential was scanned from –0.25 V to +0.25 V around the rest potential at a rate of 50 mV/sec.

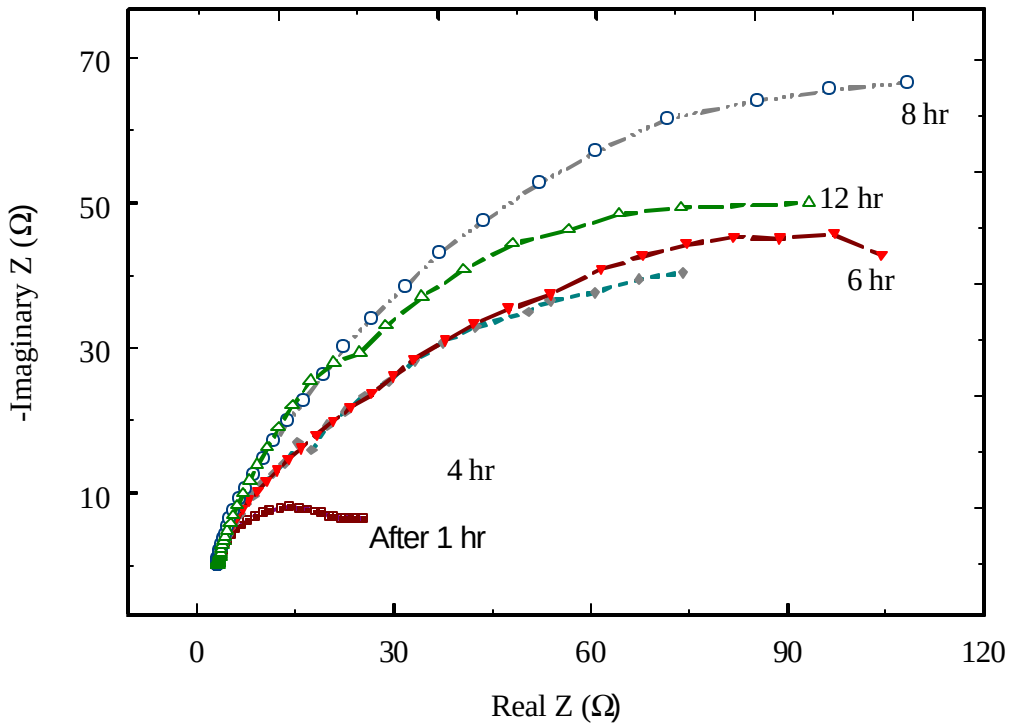

Figure 1.5a Nyquist plot of impedance response of Ni electrode in Li + Na carbonate melt at 650 ^{o}C after different times of immersion.

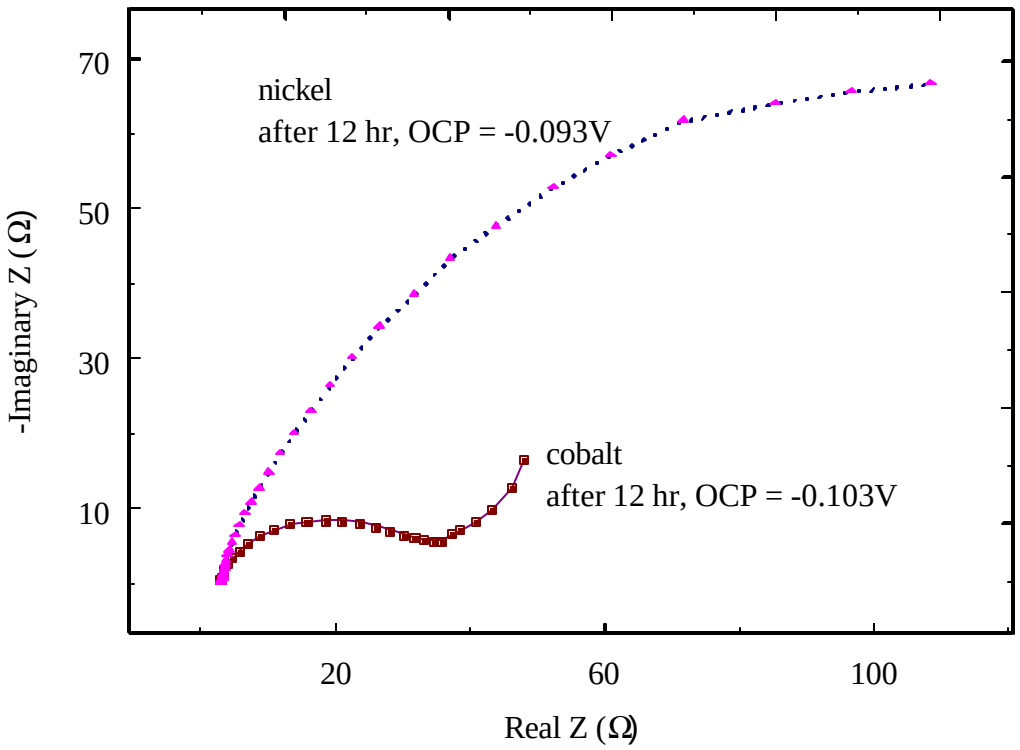

Figure 1.5b Comparison of impedance responses for Ni and Co electrodes in Li + Na carbonate melt at 650 ^{o}C after different times of immersion.

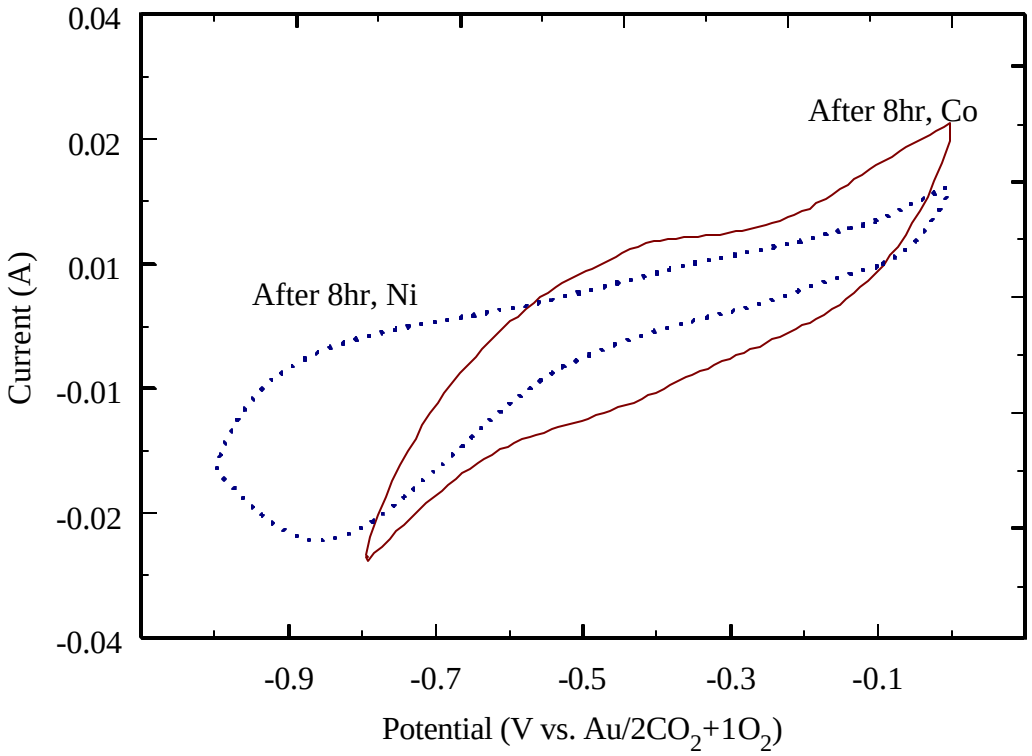

Figure 1.6 Comparison of CV responses for Ni and Co electrodes in Li + Na carbonate melt at 650 ^{o}C after eight hours of immersion.

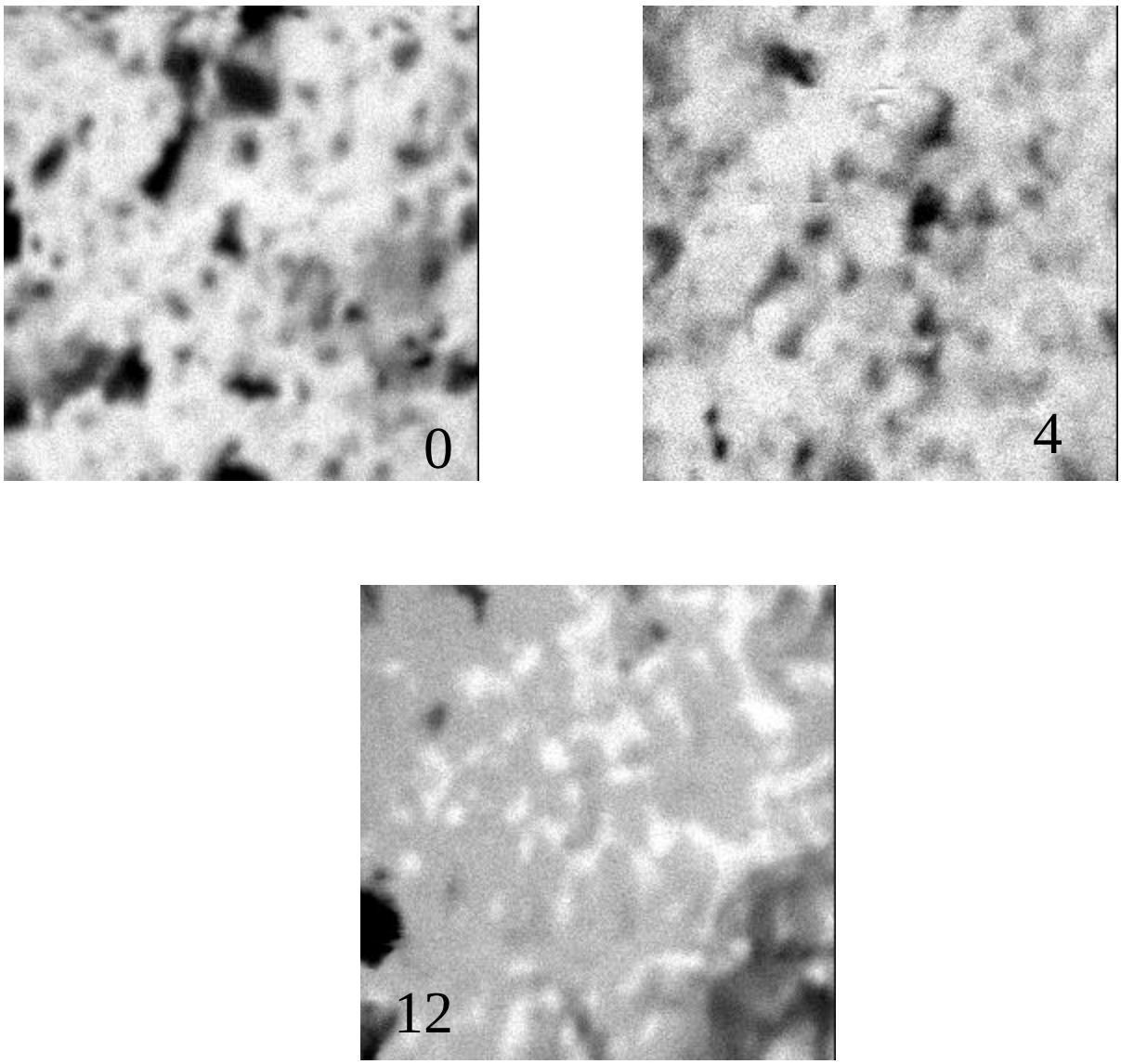

Figure 1.7 EPMA maps of *in-situ* oxidized Ni after different times of oxidation. Completely oxidized (bottom) nickel shows the presence of bivalent and trivalent nickel oxide phases.

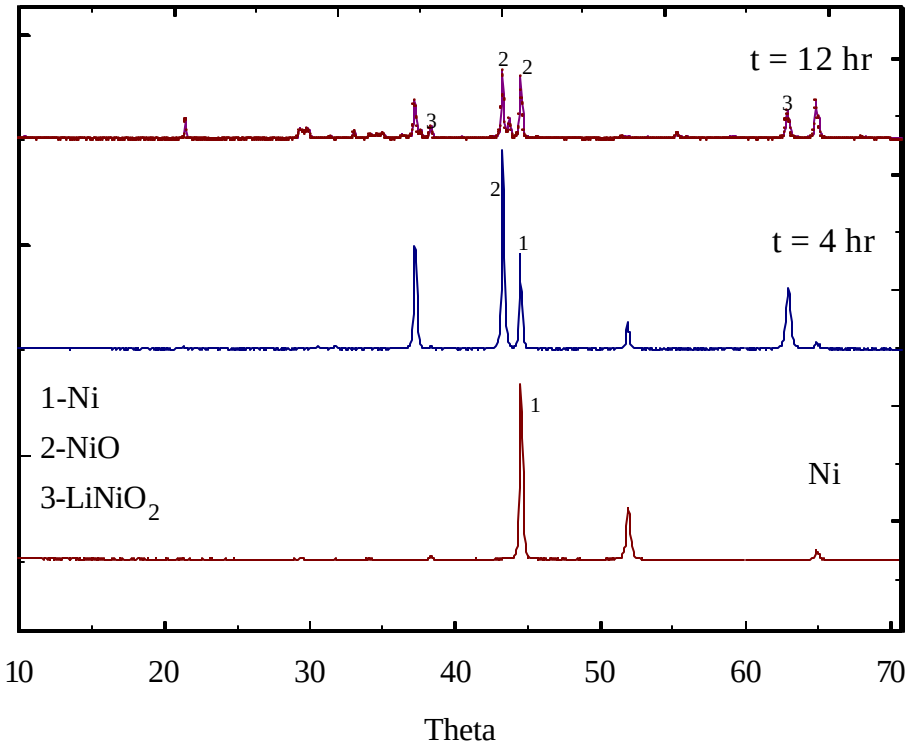

Figure 1.8 XRD patterns of fresh Ni and *in-situ* oxidized Ni after different times of oxidation

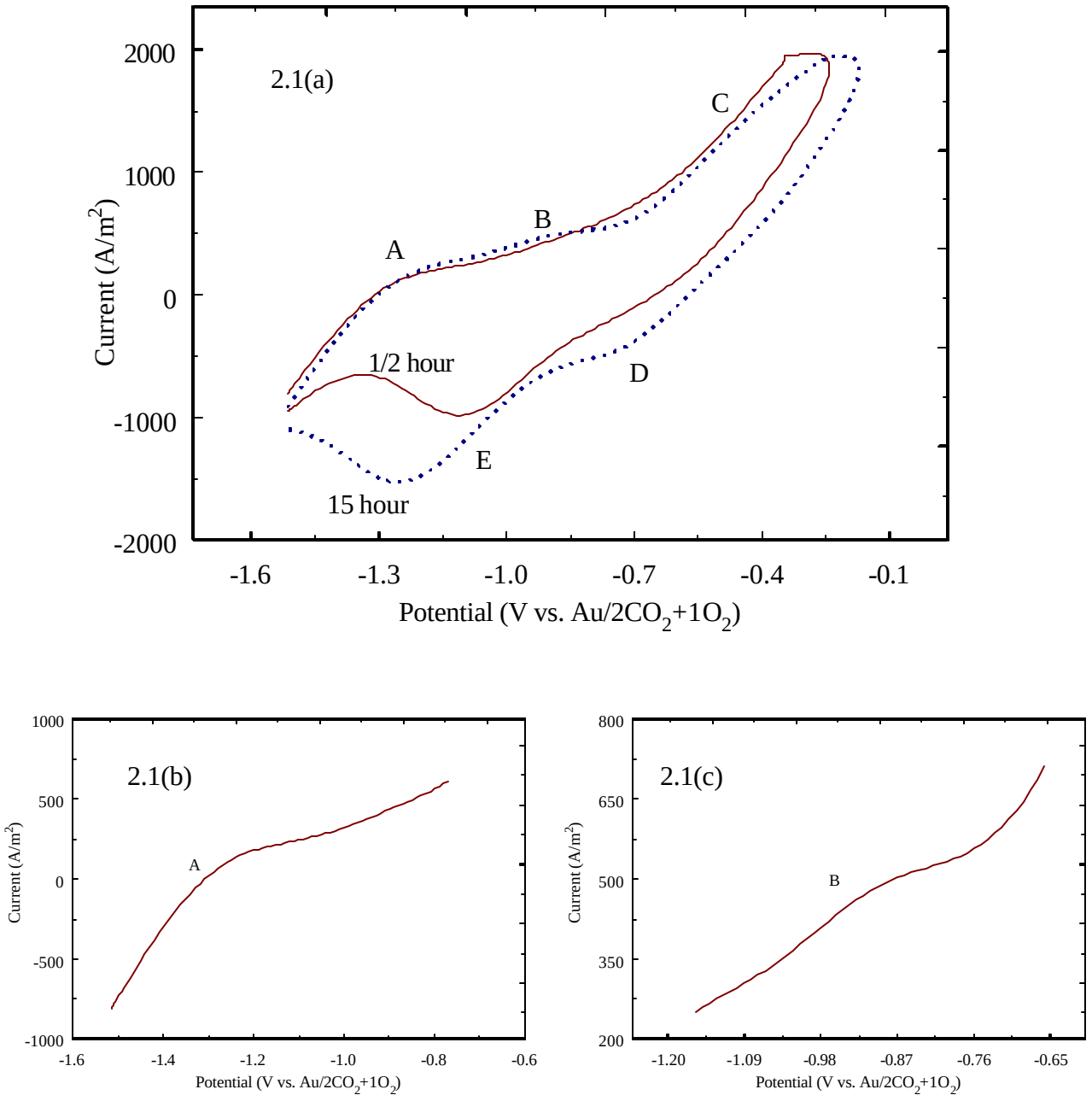

Figure 2.1 Cyclic voltammograms of 304 steel after 0.5 h and 15 h of exposure in Li + Na carbonate under cathode gas.Points A and B in 2.1(a) have been expanded and shown in 2.1 (b) and 2.1 (c) respectively.

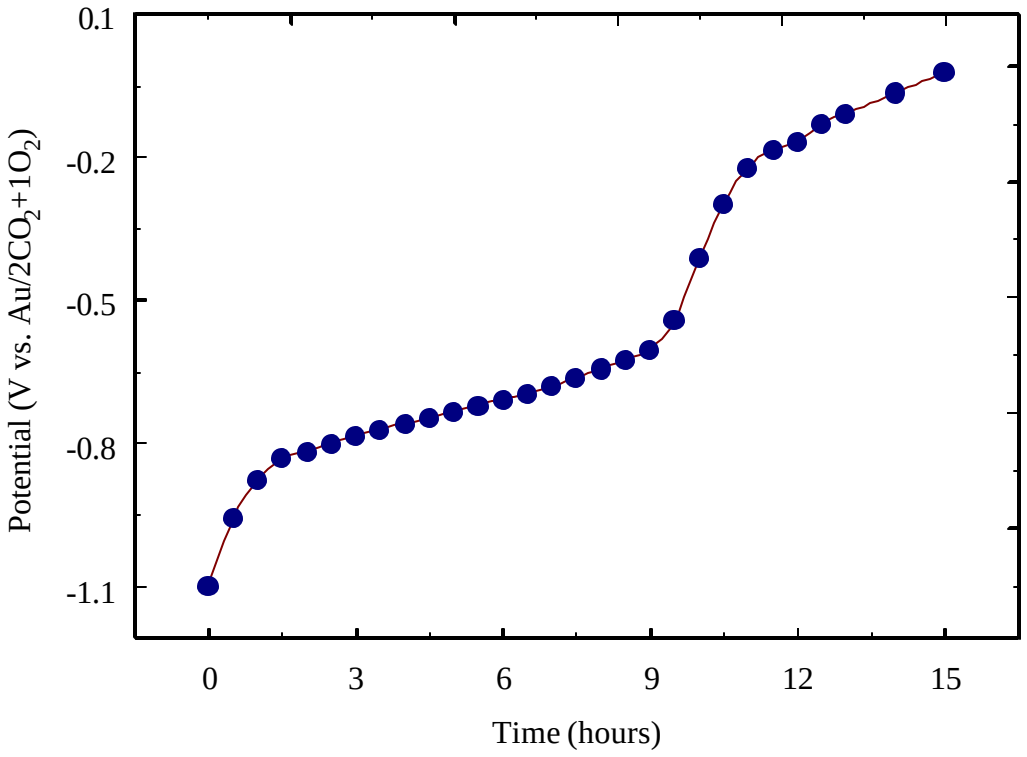

Figure 2.2 OCP of 304 steel vs. time in Li + Na carbonate under cathode gas.

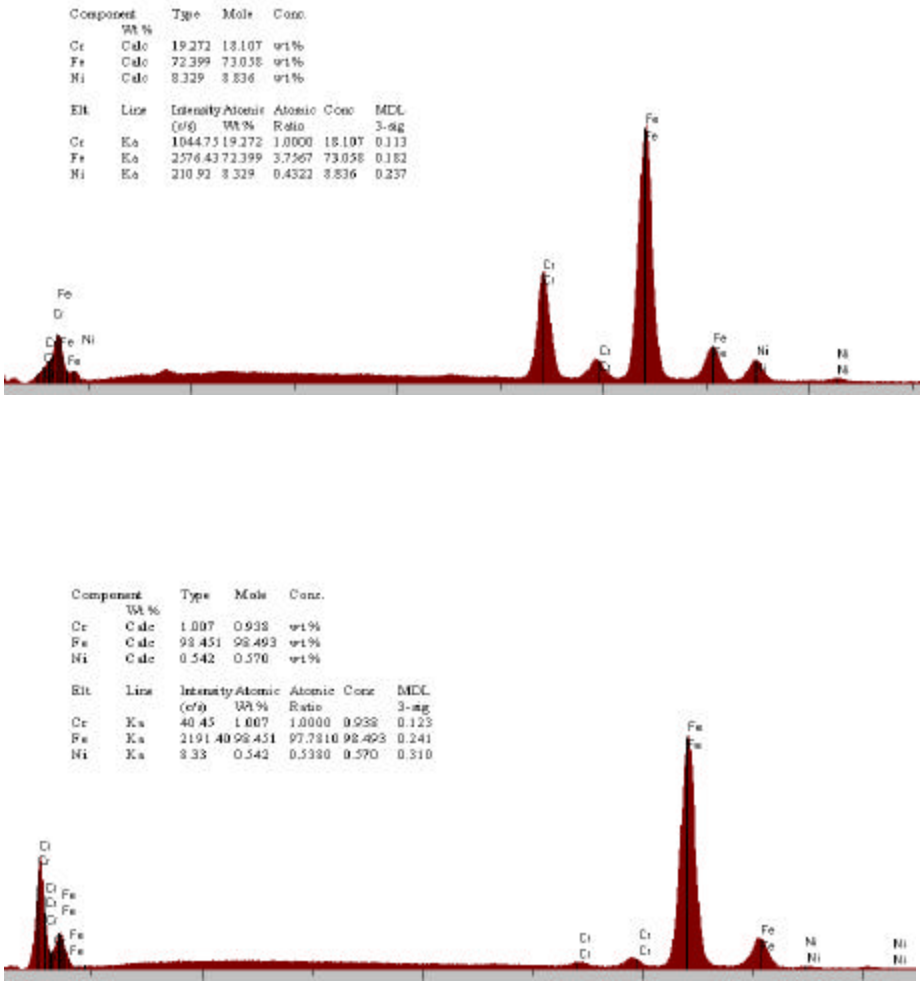

Figure 2.3 EDAX analysis for surface composition of fresh (top-a) and 304 steel oxidized (bottom-b) in Li + Na carbonate under cathode gas.

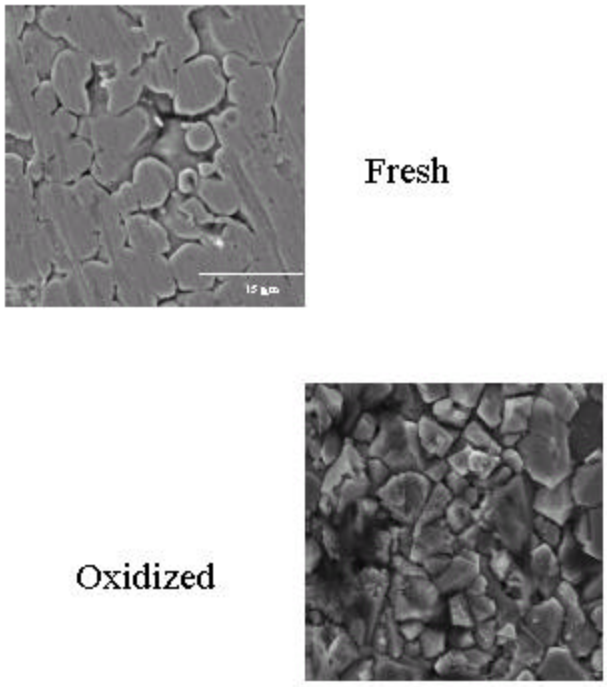

Figure 2.4 SEM micrographs of fresh (top-a) and 304 steel oxidized (bottom-b) in Li + Na carbonate under cathode gas.

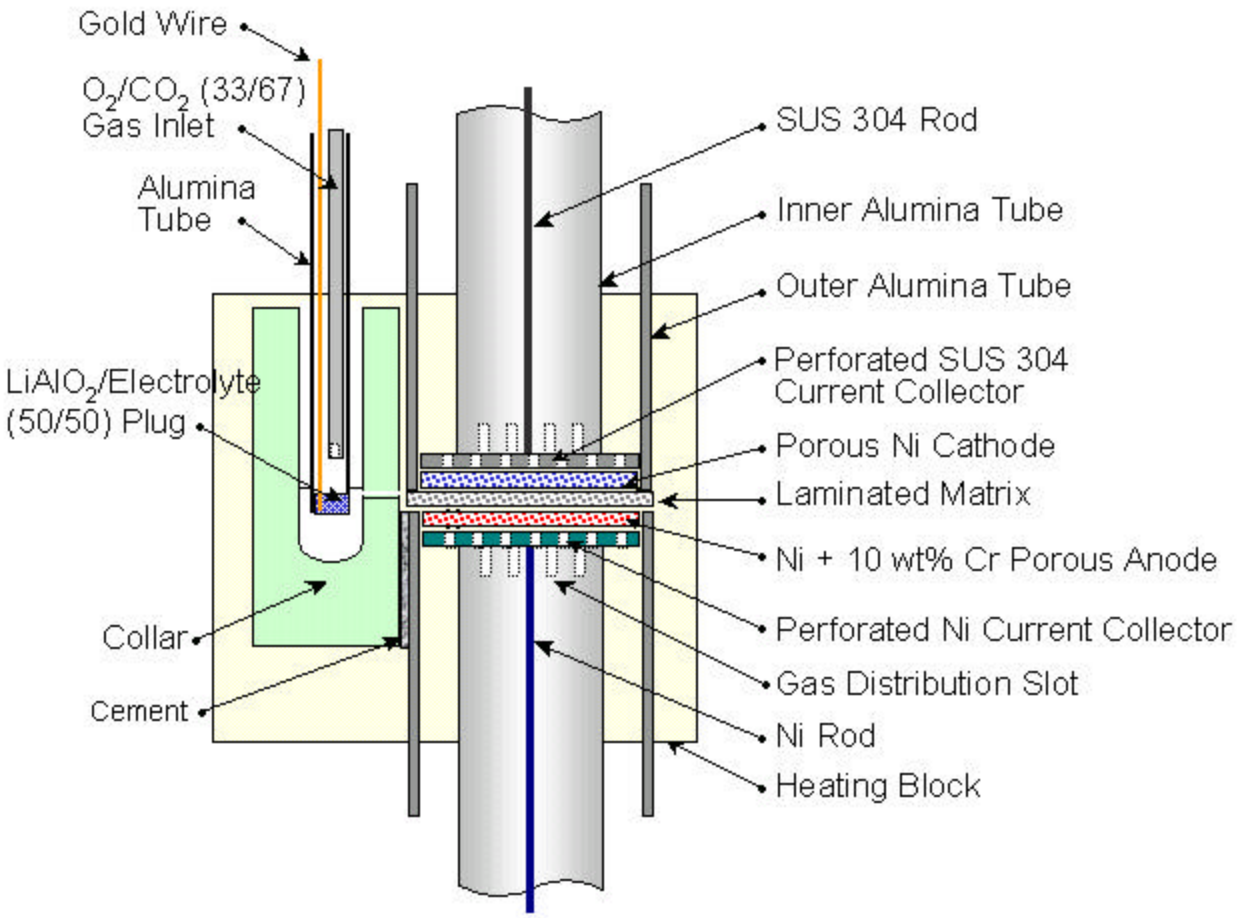

Figure 3. Design of a 3 cm^2 lab scale MCFC cell